Title	Seismic behavior of reinforced concrete interior wide-beam column joints
Author(s)	Kulkarni, Sudhakar A.; Li, Bing.
Citation	Kulkarni, S. A., & Li, B. (2009). Seismic behavior of reinforced concrete interior wide-beam column joints. Journal of Earthquake Engineering, 13(1), 80-99.
Date	2009
URL	http://hdl.handle.net/10220/8591
Rights	© 2009 A.S. Elnashai & N.N. Ambraseys. This is the author created version of a work that has been peer reviewed and accepted for publication by Journal of Earthquake Engineering, Taylor & Francis. It incorporates referee's comments but changes resulting from the publishing process, such as copyediting, structural formatting, may not be reflected in this document. The published version is available at: [DOI: http://dx.doi.org/10.1080/13632460802211941].

Seismic Behavior of Reinforced Concrete Interior Wide-Beam Column Joints

SUDHAKAR APPARAO KULKARNI and BING LI

School of Civil and Environmental Engineering, Nanyang Technological University, Singapore

In this article, experimental and finite element (FE) numerical investigations on interior wide-beam column joints are presented. The experimental research consisting of three full-scale interior wide-beam column specimens was carried out at Nanyang Technological University, Singapore to study the seismic behavior. Details of the test results are discussed to understand the specimens' seismic performance in terms of general behavior, hysteresis loops response, and strain profiles of longitudinal reinforcement. In the FE numerical study, the three-dimensional (3D) model developed is validated by comparing the analysis results with the experimental test results, which has shown a good agreement. A parametric study is performed to elucidate more information and to understand the influence of critical parameters affecting the joint behavior such as column axial load, beam anchorage ratio, and wide beam participation.

Keywords Wide Beam-Column Joint; Shear Stress; Reinforcing Detail; Drift Ratio; Finite Element; Column Axial Load; Hysteresis Loops

1. Introduction

A wide-beam system processes many advantages from the architectural and economical considerations because of its special nature. The potential benefits include reduction in formwork, simplicity of repetition thereby accelerating the construction speed, and decrease in story height leading to reduction in the cost of construction. With these and other advantages, the buildings and composite structural systems involving wide beam frames have become very popular as the gravity load-resisting frames in non seismicity regions. In the meantime, the potential advantages and applications of the wide beam systems in a lateral load-resisting structure are often ignored due to the lack of understanding of its seismic performance.

Design code BS 8110 [1997] strictly restricts the use of wide-beam column joints to resist earthquake loads. Moreover, some geometric restrictions on the elements of wide beam-column system are often imposed based on historic design practices. For instance, in New Zealand, the beam width restriction is the lesser of $b_c + 0.5h_c$ or $2b_c$, where b_c is the column width and h_c is the column depth. In the U.S., the beam width is restricted to $b_c + 1.5h_b$, where h_b is the beam depth. However, Stehle *et al.* [2001] and Siah *et al.* [2003] found that by incorporating a special type of bars detailing, no beam width limitations are required for the design of wide-beam flooring systems in regions of high seismicity. A research study by Gentry and Wight [1994] suggested a slight

Address correspondence to Sudhakar Apparao Kulkarni, School of Civil and Environmental Engineering, Nanyang Technological University, Singapore; E-mail: ksudhakar@pmail.ntu.edu.sg

relaxation in the beam width from the current ACI recommendations on wide-beam column connection: $b_b \leq b_c + 2h_c$ (where b_b is the beam width).

It was further added that the wide-beam column joints performed well even when b_w/b_c was greater than three.

Among previous studies, the primary concern for wide-beam column joints is the effectiveness of the longitudinal reinforcement that passes outside of the column core because of the different load transfer mechanism. Hatamoto *et al*. [1991] indicated that the amount of beam reinforcement placed outside of the joint core should be limited to reduce torsional stress. In addition, sufficient confinement should be provided to the outermost part of beam to improve the torsional rigidity and provide adequate anchorage for the beam reinforcement. Some investigations on wide-beam column joints also focused on lower stiffness, energy dissipating capacity, and bond slip of column bars [Ehsani and Wight, 1985; LaFave and Wight, 1999]. Recently, a series of research projects conducted by LaFave and Wight [2001] has highlighted the impact of these parameters on the behavior of wide-beam column joints. Test results showed that the energy dissipating capacity of wide-beam column joints is almost equal the conventional beam connection [LaFave and Wight, 1999, 2001].

Until now, experimental research on wide-beam column joints was not sufficient enough to fully understand their seismic behavior, while numerical investigations in these areas are very scarce. Therefore, with a aim to contribute on these research topics, the study in this article is planned in two parts: experimental and numerical investigations. In the experimental program, three test specimens were designed as per BS 8110 [1997] code provisions with some modifications to include moderate seismic detailing of reinforcement. The specimens were tested under quasi-static cyclic load reversals and their behavior was studied. However, due to the unique nature of the tested specimens, many key parameters influencing the joint behavior could not be varied. Hence, the second part of the research includes a nonlinear FE numerical study covering the validation of the numerical models against the experimental results and then, application of the models to perform the parametric investigation by varying critical parameters influencing the joint behavior.

2. Test Program

The dimensions and reinforcing details of the three specimens, designated as IWB1, IWB2, and IWB3, are shown in Fig. 1. These specimens represented a connection part of the frame obtained by terminating the beam at its mid-span and columns at their mid-heights, where the points of inflection of the bending moment diagram due to the horizontal lateral loading occur. In order to match the dimension of the test frame, the overall dimension of the specimens was scaled so that the height of the column was 2,725 mm and the span length was 4,000 mm, as shown in Fig. 1.

2.1. Description of Test Specimens

The main beam section of these specimens was 800 mm × 300 mm and the column cross-section was 900 mm × 300 mm. In Specimens IWB1 and IWB3, columns were orientated such that they would be able to bend about their strong axes, which would lead to a beam width to column width ratio b_w/b_c at 2.67, as shown in Fig.1. A transverse beam with a cross-section of 800 mm x 300 mm was cast into the joint core of these two specimens. Since the depth of the transverse beam was identical to that of the main beam, it was also a wide beam. Conversely, Specimen IWB2 could not be strictly classified as a wide beam

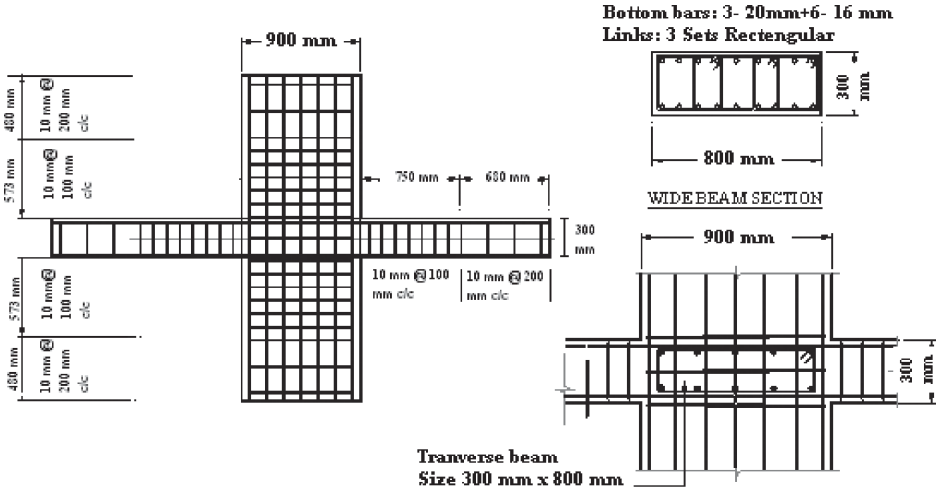

(a) Specimen IWB1 and IWB3

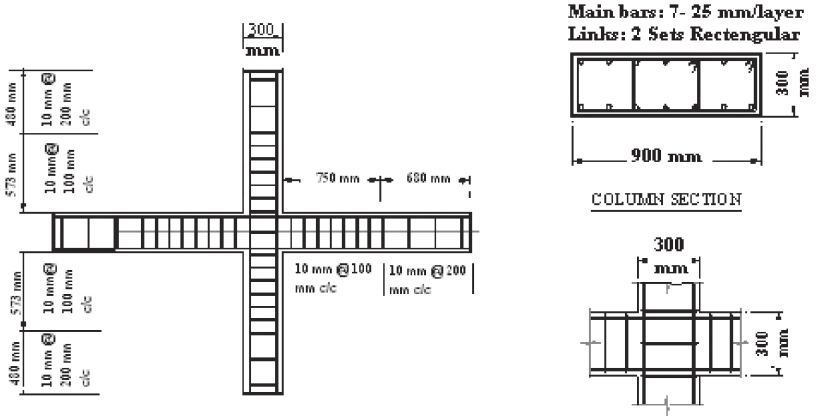

(b) Specimen IWB2

FIGURE 1 Specimen details showing dimensions and reinforcement.

because its column width was slightly wider than that of the beam giving a beam width to column width ratio at 0.89 (see Fig. 1). Since all the beam longitudinal bars of Specimen IWB2 had been anchored in the column core, a transverse beam was not necessary in this specimen.

2.2. Reinforcement Details

The reinforcing details of Specimens IWB1 and IWB3 are shown in Fig. 1a, while Fig. 1b presents the reinforcement details for Specimen IWB2. The beam sections of all wide-beam column joint specimens consisted of 3 bars of 22 mm diameter and 6 bars of 20 mm diameter as the top flexural reinforcement, whereas the bottom reinforcement was comprised of 3 bars of 20 mm diameter and 6 bars of 16 mm diameter. This made the ratios steel area of the top and bottom longitudinal reinforcement as 1.43% and 1.0% of

A_g, respectively. In the beams of Specimens IWB1 and IWB3, 3 bars of 22 mm at the top and 3 bars of 20 mm at the bottom were placed inside the column core, indicating their anchored area in the column core as 37.7% and 43.8% of the top and bottom bars, respectively. All the columns were uniformly reinforced by using a total of 14 bars of 25 mm diameter, amounting to a column reinforcing ratio of 2.54%. The longitudinal bars of the transverse beam consisted of 5 bars of 20 mm and 22 mm diameters at the top and bottom, respectively.

In Specimens IWB1 and IWB3, the column depth to beam bar diameter ratio ranged from 41–56.3. Obviously, these values were much higher than ACI 318-05 design code recommendation of 20, implying a satisfactory bond criterion. For Specimen IWB2, due to different column orientation, these values were modified to 13.6 and 15 for 22 mm and 20 mm diameter bars, respectively, indicating an inferior bond criterion as per ACI 318-05 design code recommendation. In all wide-beam column joints, the beam depth to column bar diameter ratio was 12, which was much lower than ACI 318-05 design code requirement.

2.3. Material Proprieties

Longitudinal reinforcement for the beam, columns, and transverse beams consisted of deformed bars characterized by an yield strength f_y equal to 460 MPa. Bar diameters of longitudinal reinforcement were varied from 25 mm to 16 mm. Mild steel bars of 10 mm diameter characterized by an yield strength f_y equal to 250 MPa were used for transverse reinforcement while joint shear reinforcement consisted of 16 mm diameter deformed bars. Compressive strength of concrete targeted during the design was 70 MPa for Specimens IWB1 and IWB2, and 40 MPa for Specimen IEW3. A lower grade of concrete in Specimen IWB3 was intended to investigate the concrete strength behavior on the joint performance. The average compressive strength of concrete, f'_c, obtained from the concrete cylinder samples, was found equal to 64.3 MPa, 66.4 MPa, and 47.9 MPa, for Specimens IWB1, IWB2, and IWB3, respectively.

2.4. Nominal Capacities

The design parameters of the specimens such as the horizontal lateral load, column to beam moment ratio, joint shear force, etc., were estimated using the material properties obtained from the tests, and following the recommendation of ACI-ASCE Committee 352. Table 1 summarizes the results of the expected capacities. It can be seen that all specimens were designed following the philosophy of ''strong column and weak beam.'' The minimum column to beam moment ratio, which is 1.4 as per ACI-ASCE Committee 352 requirement, was satisfied.

TABLE 1 Design parameters

Specimen	P_{th} (kN)	Moment ratio		Joint shear force (kN)	γ	$\Delta y_{,th}$ (mm)	K_{th} (kN/mm)
IWB1	249	4.30	5.99	45.14	25.4	5.3	47
IWB2	207	1.41	1.97	50.28	37.0	6.2	33.4
IWB3	244	4.30	5.95	45.14	28.6	6.2	39.4

2.5. Test Setup

Figure 2 shows the test setup. Each of the test specimens was subjected to quasi-static load reversals that simulated earthquake loading. The bottom of the column was pinned to the strong floor of laboratory and ends of the beams were connected to this strong floor by steel links which permitted only rotation and free horizontal movement of the beam. A reversible horizontal load was applied to the column using a double acting 1,000 kN (224.8 kip) capacity hydraulic actuator. The cyclic loading history showing applied cycles versus the story drift ratio (DR) is shown in Fig. 3.

3. Experimental Results and Observations

All the specimens were applied with the displacement controlled quasi-static load reversals. The following sections describe the experimental results and observations of the tested specimens.

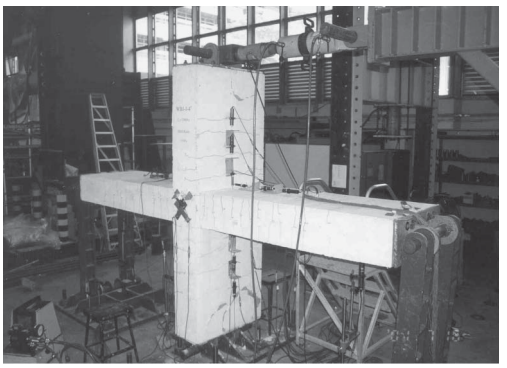

FIGURE 2 Test setup showing Specimen IWB2.

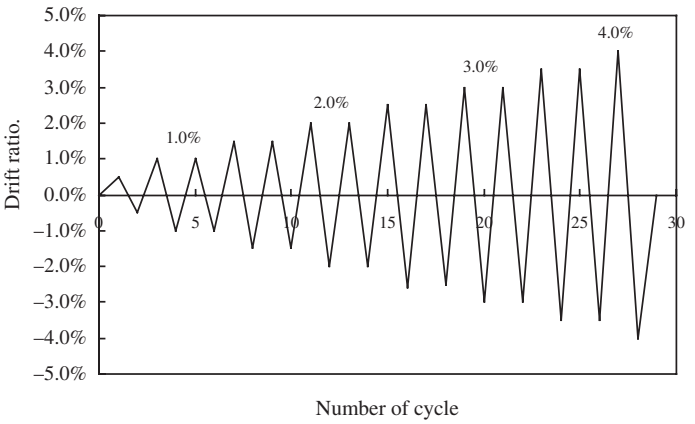

FIGURE 3 Cyclic loading history.

3.1. Specimens IWB1 and IWB3

The hysteresis loops of the shear force versus the horizontal displacement of Specimens IWB1 and IWB3 are shown in Figs. 4 and 5, respectively. The theoretical load capacities are also shown on these figures for comparison. Due to different values of concrete compressive strengths, theoretical strength of Specimen IWB1 was slightly higher than that of Specimen IWB3. However, evidently, the concrete strength did not much affect the performance of the specimens.

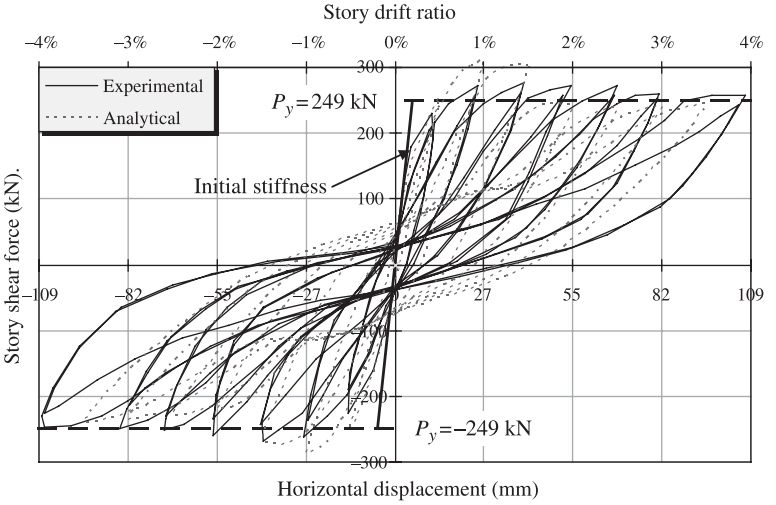

FIGURE 4 Comparison of hysteresis loops between the experimental tests and those predicted by numerical analysis for Specimen IWB1.

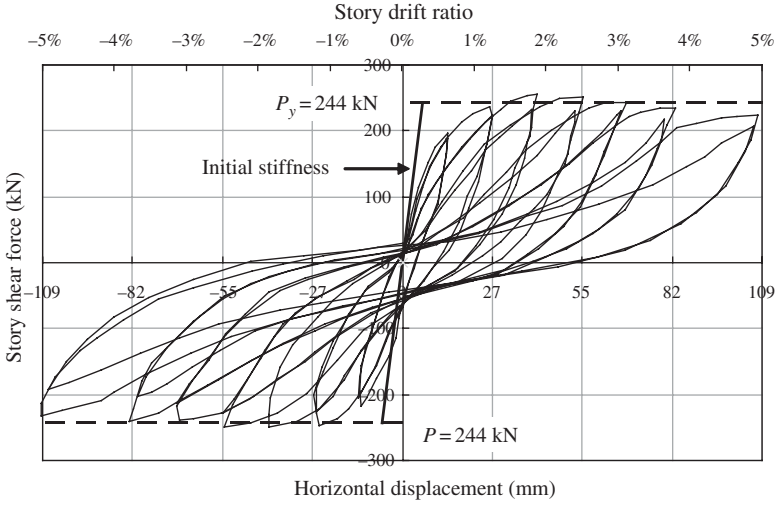

FIGURE 5 Hysteresis loops showing story shear force versus horizontal displacement for Specimen IWB3.

Figure 4 shows the hysteresis loops of story shear force versus column top displacement for Specimen IWB1. The specimen attained its calculated strength at a DR of 1.5% in both the loading directions. In the subsequent loading cycles, corresponding to a DR of 2.0%, the specimen reached its ultimate strength. It attainted the maximum strengths of 272 kN and 269 kN during the positive and negative loading cycles, respectively. In the last loading cycle, the specimen carried the strength approximately 88% of its maximum load carrying capacity. The hysteresis loops exhibited a good pinching behavior throughout the test (see Fig. 4).

As shown by Fig. 5, Specimen IWB3 attained its theoretical capacity corresponding to a DR of 1.0% in both the loading directions. The maximum capacity was obtained when the DR was 1.5%, with the value being approximately 256 kN in the positive loading direction, indicating an over-strength factor of about 4.9%. While in the negative loading direction, the maximum capacity gained was about 248 kN. In the following loading cycles, although the specimen experienced progressive reduction in its load-carrying capacity, the strength degradation was not significantly high. The hysteresis loops of the specimen showed a substantial pinching in their behavior. At the end of the test, the specimen recorded a residual load-carrying capacity of 220 kN.

Figure 6 shows the cracking pattern of Specimen IWB1. The beams experienced flexural cracking early beginning from a DR of 0.5%. With an increase in loading run to a DR of 1.0%, the existing flexural cracks propagated through the beam thickness and a few new cracks also developed along the beam span. At this stage, the specimen did not exhibit significant pinching as shown by the hysteresis loops. When the loading reached to a DR of 3%, more flexural cracks appeared in the beams and some two-way diagonal cracks were also generated. A moderate deterioration of bond along the column

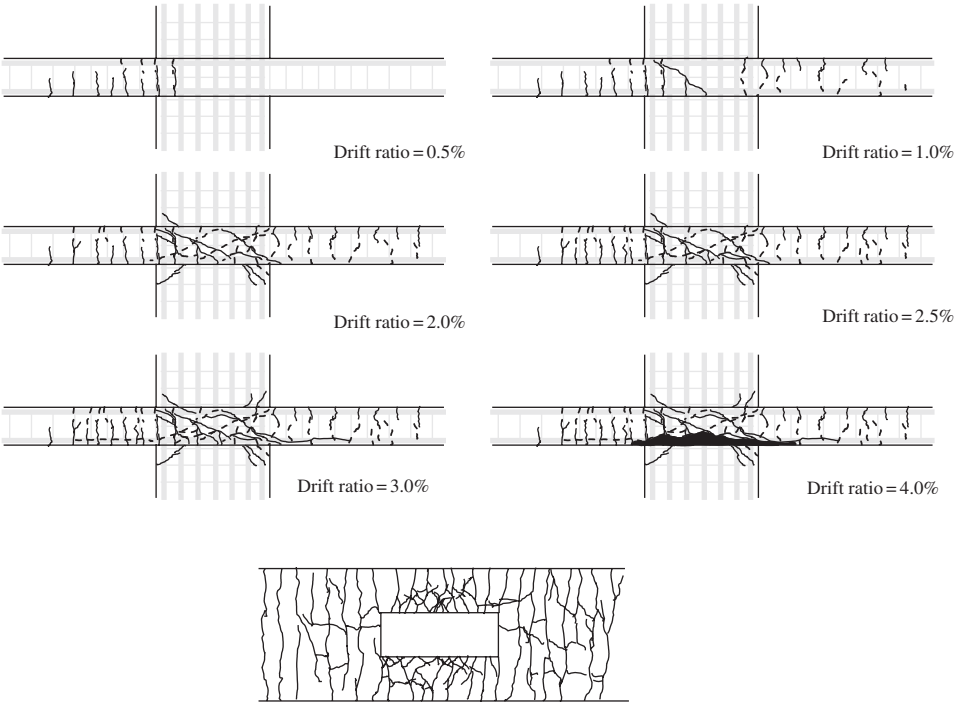

FIGURE 6 Cracking pattern of Specimen IWB1.

reinforcement within the joint core was initiated at the second loading cycle and increased progressively up to a DR of 3.0%. The column faces near the wide beams experienced minor inclined cracking, while no flexural cracking was observed in them. Finally, when the specimen was loaded to 4% DR, the specimen experienced substantial cracking coupled with spalling of concrete.

Figure 8 shows the strain profiles of the top and bottom reinforcement of the beams for Specimen IWB1. Beginning from a DR of 1.0%, the top and bottom bars experienced the yielding. At this stage, the maximum bond stress obtained along the top and bottom reinforcements were 6.37 MPa and 4.46 MPa, respectively.

Generally, the cracking pattern of Specimen IWB3 was analogous to Specimen IWB1, as shown in Fig. 7. On the wide beams of Specimen IWB3, flexural cracking was initiated early corresponding to a DR of 0.5%. As the DR reached to 1.0%, these cracks propagated along the beam depth and also spread along the beam span. In the subsequent loading cycles between DRs of 2.0% and 3%, the beam flexural cracks evenly spread over three-fourths of the beam span. However, no shear cracking was detected throughout the test. The upper and lower faces of the columns developed some minor

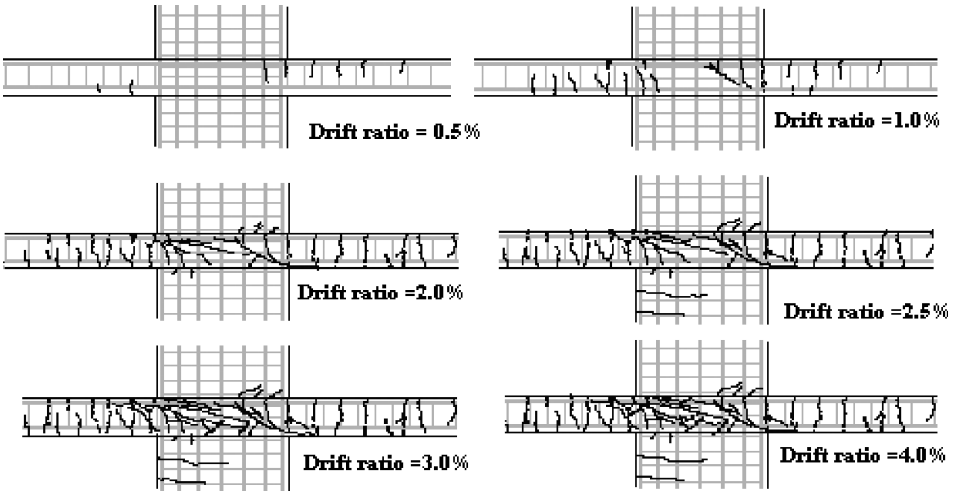

FIGURE 7 Cracking pattern of Specimen IWB3.

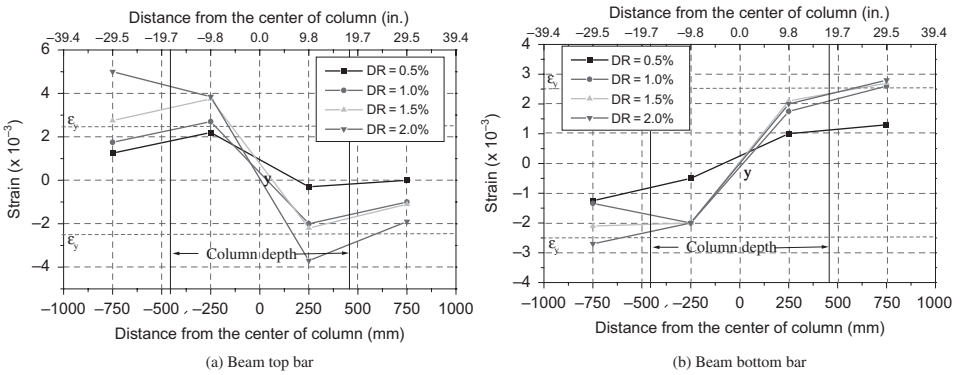

FIGURE 8 Strain profiles of beam reinforcement, Specimen IWB1.

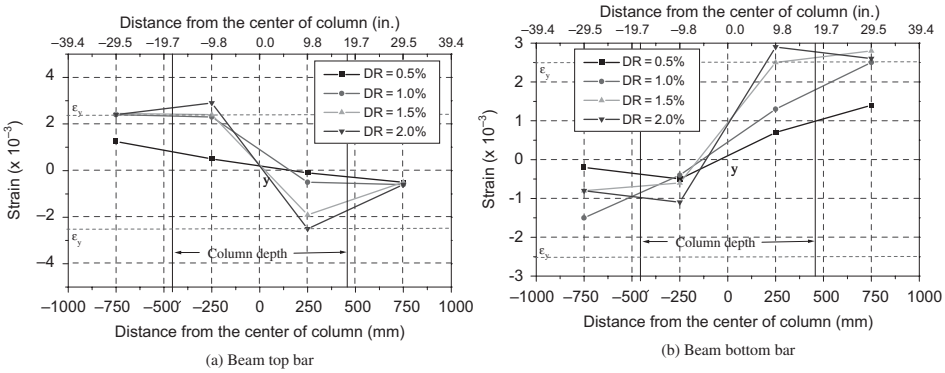

FIGURE 9 Strain profiles of beam reinforcement, Specimen IWB3.

cracks, while a part of the lower column adjacent to the joint region experienced moderate bond splitting.

The strain profiles of the top and bottom reinforcement of the beam for Specimen IWB3 is presented in Fig. 9. At a DR of 1.5%, the first yielding of the top and bottom bars occurred. The maximum bond stress values obtained along the top and bottom reinforcements of the beams were 4.93 MPa and 3.14 MPa, respectively. Throughout the test, rebars of the columns of Specimens IWB1 and IWB3 exhibited an elastic behavior.

3.2. Specimen IWB2

Figure 10 shows the hysteresis loops of shear force versus horizontal displacement for Specimen IWB2. The specimen attained its theoretical capacity corresponding to a DR of around 1.0% in both the loading directions. At a DR of 1.5%, the specimen gained its maximum capacity of 215 kN in the positive loading direction indicating a limited over-strength factor of about 3.8%. In the following loading cycles, the strength of the

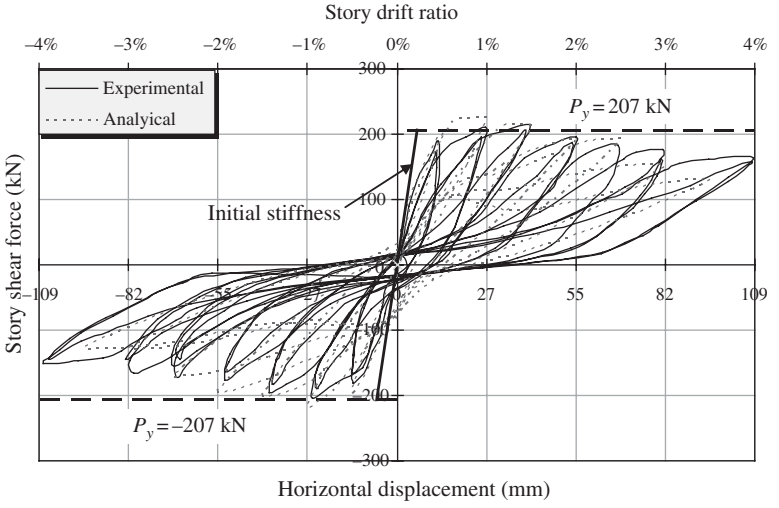

FIGURE 10 Comparison of hysteresis loops between the experimental tests and those predicted by numerical analysis for Specimen IWB2.

specimen decreased progressively and, finally, reached a residual load-carrying capacity of 164 kN and 152 kN, respectively, in the positive and negative loading directions.

The cracking pattern of the specimen is presented in Fig. 11. In the wide beams and columns, flexural cracks appeared early corresponding to a DR of 0.5% and continued up to a DR of 1.0%. At this stage, a few cracks extending the full depth of the beams and columns were also detected. In the subsequent loading cycles up to a DR of 3.0%, flexural cracking spread significantly along the full length of beam span. On the columns, the flexural cracks spread over three-fourths the height of the columns.

Figure 12 shows the strain profiles of the top and bottom reinforcement of the beams for Specimen IWB2. The strains in all the top and bottom longitudinal reinforcements of beams

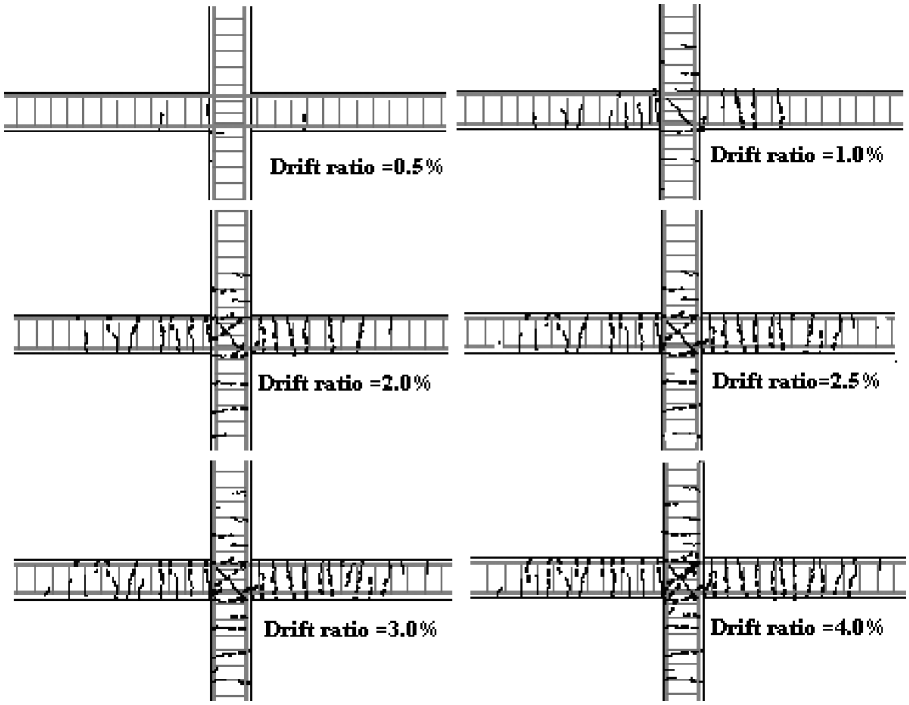

FIGURE 11 Cracking pattern of Specimen IWB2.

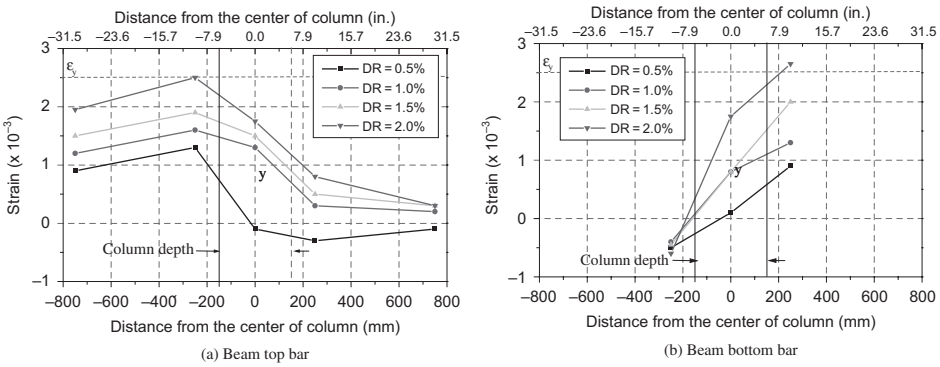

FIGURE 12 Strain profiles of beam reinforcement, Specimen IWB2.

increased rapidly beginning from a DR of 1.0%, while no yielding was observed at this stage. At a DR of approximately 2.5%, the bottom reinforcement of the beams yielded, while the top layer reached the yield strain at a DR of 2.0%. The maximum bond stress of 7.53 MPa and 8.45 MPa were obtained along the top and bottom reinforcements, respectively.

4. Discussion on Experimental Observations

4.1. Loading Capacity and Hysteretic Responses

The story shear force versus the horizontal displacement relationships showed that all the interior wide-beam column specimens had adequate load-carrying capacities. Especially, Specimens IWB1 and IWB3 presented limited over-strength behavior with their respective maximum capacities being about 11.2% and 4.9% higher than the theoretical predictions. However, Specimen IWB2 did not show any strength enhancement.

It was noticed that the specimens reached their nominal capacities at relatively higher DRs, that is, approximately 1.5% or above. This was mainly due to the flexibility of the specimens, which could be attributed to the lower stiffness of the shallow wide beams. The early bond slipping in both beam and column longitudinal bars made the specimens more flexible. During the test, the specimens experienced stiffness degradation and pinching of hysteresis loops, which is a typical phenomenon in a RC structure.

4.2. Influence of Design Parameters

A research study by Stehle *et al*. [2001] suggested that the width ratio is not the most critical design parameter in the design of wide beam systems. Comparison of the test results of Specimen IWB2 with those of Specimens IWB1 or IWB3, it was found that the lower width ratio of Specimen IWB2 did not much help to improve the response. In contrast, Specimens IWB1 and IWB3 exhibited a better performance with respect to Specimen IWB2. Therefore, the design recommendation on the beam to column width ratio cannot guarantee the performance by itself. More studies are suggested to determine an appropriate beam to column width ratio of wide-beam column system.

4.3. Column Behavior

Specimen IWB2 meets ASC-AICE Committee 352 recommendation on column to beam flexural ratio, which is 1.4. Therefore the ''Strong Column and Weak Beam'' philosophy was satisfied. In comparison with this specimen, the column to beam flexural strength ratio of Specimens IWB1 and IWB3 was extremely high. As summarized in Table 1 the ratios are 4.3 and 5.9 in the positive and negative loading directions, respectively. This led to a very low strain level in the column reinforcements maintaining elastic response of the columns. From the column bars strain profiles, it can be seen that most of the column bars did not yield during the test. The requirement of ''Strong column and weak beam'' is aimed at preventing the column hinges mechanism occurred during the earthquake. However, extremely large flexural ratio is not an economical design solution.

During the test, signs of bond deterioration were detected in the column reinforcements for all six specimens. To limit the bond stress within the joint, a Bond Index (*BI*) by Kitayama *et al*. [1991] was introduced:

$$BI = \frac{u_b}{\sqrt{f'_c}} = \frac{f_y(d_c/h_c)}{2\sqrt{f'_c}}, \quad (1)$$

where u_b is the maximum bond stress of column reinforcement over the beam depth, d_b is the beam bar diameter, h_c is the column depth, f_y is the yield strength of beam bars, and f'_c is the concrete compressive strength. Bond index for column bars can also be computed using Eq. (1). In this testing program, all the three specimens had an uniform beam depth and column bar diameter. Therefore, an uniform column *BI* can be obtained for all the specimens and was equal to 2.35 (in MPa units). This value was extremely larger than the Japanese recommend limit, which is 1.4 (in MPa units). The computed *BI* was based on the measured maximum bond stress on column within the joint and was never greater than 2.35. However, some of these values were larger than the Japanese recommended limit. In all specimens, the column reinforcement in the top and bottom of the joint region experienced tensile strain, indicating the fact that a smooth transition from tension to compression could not take place over the column depth.

4.4. Beam Behavior

The observed yielding pattern of wide beam longitudinal reinforcement in all specimens indicated that there could be a delay in the development of a full-width plastic hinge in wide beams. In specimens IWB1 and IWB3, the top reinforcement in the beams placed outside of the column core did not yield during the test. Comparison of strains in the outmost rebars and those rebars passing through the column showed a different strain history. The strain histories for the bottom bars passing away from, and through, the mid-depth of the column were very similar. The yielding of bars located in the outermost regions of the wide beams indicated the development of full-width hinge, which happened when the specimens reached higher loading levels. The bottom bar strain history also indicated a strain lag among the different reinforcements. The delay of plastic hinge development was dependent on the bond condition and the confinement of the reinforcement in the outside region of the joint. The specimens were not provided with any extra beam links outside region of the column.

In general, wide beam reinforcement had more favorable bond condition than column bars, as measured by the h/d_b and the bond index. In addition, the overall bond response of the wide beam bars was better than that of the column bars. The data recorded during the tests showed that bond deterioration of bars passing outside the column core was faster than the bars passing through it. This was due to the fact that the beam reinforcement placed outside the column region had no extra hooks to provide adequate confinement to the concrete. Shear force carried by the wide beams was generally lower compared with a normal depth beam-column specimen. The wide beams of the specimens never exhibited any inclined cracking which can be attributed to excessively high shear strength of the beams. Therefore, beam shear reinforcement can be relaxed.

4.5. Joint Shear Behavior

According to ASC-AICE Committee 352 recommendation, the joint shear is resisted mainly by the concrete strut mechanism rather than the truss mechanism, unless a good bond condition is provided within the joint. Table 1 shows the level of shear strength calculated following ASC-AICE Committee 352 recommendation, and assuming that the joint area is equal to the column section. Compared with this limit, the shear level

associated with the shear deformations were probably low. Similar findings were also indicated during investigations by other researchers [Ehsani and White, 1985; Bonacci and Pantazopoulou, 1993]. Therefore, joint shear requirement could be relaxed for wide-beam column frames.

The joint core of the specimens was confined by using the joint transverse reinforcement. Links located at the middle level of the joint generally showed the largest stain response. Most of the joint shear was carried by the concrete strut mechanism during the early stages. After the joint shear cracking generated, the concrete strut mechanism could not carry the force alone, and hence, it was required by the shear reinforcement to carry a major portion of the shear force. However, until the final loading stage, none of the joint links reached the yield strain, irrespective of the nature of force (tensile or compressive) that existed in them. This may be attributed to the large effective joint shear area and the confinements from the column longitudinal reinforcements and transverse beam. The test results also indicated that the joint shear strength of the test specimens was enough to withstand the imposed deformation history. No sign of shear distress was noticeable from the load versus displacement histories during the test.

5. Finite Element Analysis

Although the experimental research revealed extensive details about the interior wide beam-column joints, effects of many critical parameters like the column axial load, bar anchorage ratio, etc., could not be varied. Therefore, to further enhance the understanding of complex behavior of the wide beam-column joints, the following sections present a nonlinear FE numerical investigation. In this study, the specimens were modeled using a 3D modeling technique. A 3D modeling helps in accurately defining the geometry of a specimen and properly positioning of rebars in it. Besides, the complex nature of stresses at various key sections such as around the columns, inside the joint and on the top of wide beams, can be clearly studied using a 3D analysis.

5.1. Material Modeling

In material modeling, the model of concrete was based on nonlinear fracture theory to account for cracking, while plasticity models were used for concrete in compression and reinforcing steel. The details of concrete material modeling in elastic-plastic state, cracked concrete options in tension, and compression can be found in Kulkarni *et al*. [2008]. The von Mises yield criterion with isotropic strain hardening and an associated flow rule were used to describe the constitutive behavior of the reinforcement. The bars were modeled with the DIANA options of either embedded reinforcements or according to the recommendations of separate truss elements. The stress-strain relationship (elasto-plastic curve) of reinforcing steel can be referred in the literature [Kulkarni *et al*., 2008].

5.2. Bond Slip Theory and Element Description

Bond between concrete and reinforcing steel significantly influence the overall response of a RC structure due to its effects such as localized failures, loss of energy dissipation, etc. The pinching of hysteresis loops was caused by closing and opening of cracks or debonding of reinforcing steel. In order to have a realistic numerical response of a RC structure, therefore, addressing the interaction between steel and concrete is very important. A brief description of the bond slip model incorporated in the FE numerical study is summarized in the following sections.

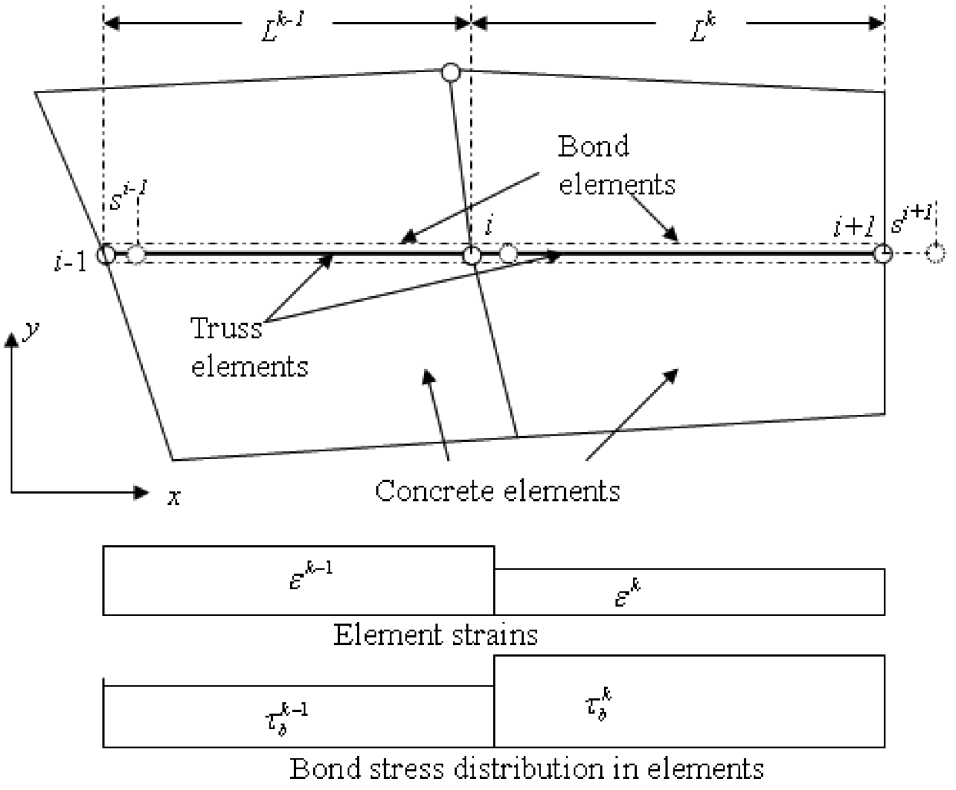

FIGURE 13 Description of bond element.

Figure 13 shows the arrangement of truss and bond elements embedded in concrete elements. In the formulation, the concrete is treated as a 2D or 3D continuum element, while the truss and bond elements are assumed to be of constant strain and constant slip, respectively. For bond element, a new degree of element s is introduced to represent the bond slip. At i^{th} node of the element boundary, s^i is the difference between concrete and bar displacements. The nodal displacement for the truss element at i^{th} node can be calculated as:

$$\tilde{u}^i = u^i + s^i. \tag{2}$$

If L^k is the length of truss element k and E is the Young's modulus of the truss element, the stress in truss element k with nodes i and $i+1$ can be evaluated as:

$$\sigma^k = \frac{E}{L^k}\left(\tilde{u}^{i+1} - \tilde{u}^i\right) = E\frac{\left(u^{i+1} + s^{i+1} - u^i - s^i\right)}{L^k}. \tag{3}$$

In order to ascertain a satisfactory bond between concrete and reinforcement bar, the equilibrium condition is given by:

$$\frac{\partial \sigma}{\partial x} \leq \tau_{b,\max}\frac{p}{A}, \tag{4}$$

where $\tau_{b,\max}$ is the maximum bond stress that can be transmitted across the interface for slip, which is analogous to friction law. p and A are the perimeter and cross-sectional area of the reinforcement bar, respectively. A bond slip is assumed to occur, if the equilibrium condition in Eq. (4) is unsatisfied. Discretizing Eq. (4) and use of constant strain condition of the truss element, it is modified to:

$$A(\sigma^{k+1} - \sigma^{k}) \leq L^{k} p \tau_{b,amx}. \tag{5}$$

A set of nonlinear simultaneous equations is formed extending Eq. (5) to all nodes of the bond elements. The nonlinear nature of the equations is due to the material nonlinearity accounted in the problem. These equations are solved using an iterative procedure and the bond slip s^{i} at all nodes is estimated. Substituting the bond slip values in Eq. (2) element stresses can be calculated. Owing to the constant strain type of truss element chosen, these stresses at the adjacent elements of a node differ. To overcome this problem, the cohesion stress τ_c surrounding the truss element is calculated using the weighted nodal stresses:

$$\tau_c = \frac{\left(\tilde{\sigma}^{i+1} - \tilde{\sigma}^{i}\right)A}{pL^{k}} \tag{6}$$

in which the weighted nodal stress $\tilde{\sigma}^{i}$ at i^{th} node of an element is estimated as given below:

$$\tilde{\sigma}^{i} = \frac{\sigma^{k} L^{k} + \sigma^{k-1} L^{k-1}}{L^{k} + L^{k-1}}. \tag{7}$$

The bond law used in the analysis is based on CEB-FIP Model Code-1990. The model parameters depend on the properties of the bar surface can refereed from the CEB-FIP Model Code-1990.

5.3. Geometry Modeling

The specimens were modeled and analyzed using the DIANA software. The concrete was modeled using 20-node 3D quadratic solid elements while the reinforcing bars were modeled as truss elements. The FE discretisation of Specimens IWB1 and IWB2 is shown in Fig. 14.

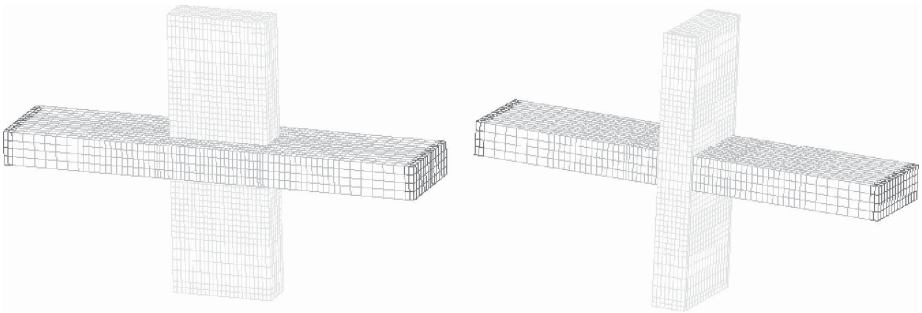

(a) (b)

FIGURE 14 Finite element modeling of the specimens (a) Specimen IWB1; (b) Specimen IWB2.

5.4. Validation of Finite Element Models

In order to verify the FE models, the analysis results were compared with the experimental test results. Because of the geometrical similarities between Specimens IWB1 and IWB3, only the results of Specimens IWB1 and IWB2 have been presented. Figure 4 illustrates the comparison of hysteresis behavior between the FE numerical and the experimental results of Specimen IWB1. A good agreement in the overall global behavior of between the experimental and numerical specimens can be observed from the figure. In the analysis, the theoretical capacity was reached corresponding to a DR of 0.5% in the negative loading direction, whereas in the positive loading direction, it did not reach the theoretical capacity. The numerical results gained the maximum capacities of 308 kN and 286 kN in the positive and negative loading directions, respectively. This indicated that at early stages, the stiffness of the numerical specimen was higher compared with its experimental counterpart by around 17.5% and 8% in the positive and negative loading directions, respectively. The specimen showed the strength and stiffness degradations in both loading directions, after reaching the maximum capacities. A good pinching behavior in the hysteresis loops, which had been observed during the experimental test, was also captured of the numerical model. Figure 10 indicates the comparison of hysteresis loops between the numerical and experimental models of Specimen IWB2. Throughout the test, the story shear strength attained by the numerical model was slightly higher compared with the experimental observations. The maximum story shear capacities predicted by the FE analysis corresponding to a DR of 1.0% were 217 kN and 211 kN in the positive and negative directions, respectively. These values were higher compared with the experimental results by approximately 6% and 4% in the positive and negative loading directions, respectively.

The strain distributions from the experimental observations showed a good agreement with those of the FE numerical predictions. The observed strain distribution in the longitudinal reinforcement of the column core was slightly higher than that of the bars passing through the outermost portions of the beams. Comparison of these results with the FE predictions showed similar trends with a few exceptions. The maximum strains in the beam reinforcement occurred at the column faces, which were also reflected in the FE analysis results. Due to the poor anchorage condition between the bars and surrounding concrete, the outermost beam bars could not properly transfer the tensile forces into the column, which reflected by the numerical and experimental results with a low-level strain distribution in those regions. The strains predicted in the beam longitudinal reinforcement were slightly greater than the measured values with yield penetration being observed in the joint core. Comparison of shear forces between the FE analysis and the experimental test results also showed a good agreement. The aforementioned facts clearly indicated that the FE predictions are capable of producing fairly accurate predictions of joint performances.

6. Parametric Studies

To elucidate more information about the complex behavior of the wide-beam column joints, the following sections present a parametric investigation. The structural response of the joints was studied by varying some key parameters such as column axial loading, beam longitudinal bar anchorage ratio, and wide-beam participation.

6.1. Influence of Column Axial Load

Paulay *et al.* [1978] and Paulay and Park [1984] were the first to investigate the effect of column axial load on the performance of beam-column joints. Thereafter, although

researchers have made efforts to understand its influence on joint shear strength and bond resistance of beam reinforcement, the optimum column load ratio is not clearly known [Kitayama *et al*., 1991; Shiohara, 1998]. According to NZS-3101, the contribution of the main strut mechanism is ignored unless a significant amount of column axial load (i.e., greater than $0.1f_c'A_g$) exists.

In this investigation, the influence of column axial load on the seismic behavior of the wide beam-column joint was studied using the FE analyses. The same loading histories as those used in the experimental tests of the specimens were applied, and the corresponding story shears versus horizontal displacements under different axial loading levels are plotted (see Figs. 15 and 16). The column axial applied varied in magnitude ranging from zero to $0.5f_c'A_g$. As observed by Fig. 15, the story shears of Specimen IWB1 increased by around 9% and 12%, as the axial load was enhanced to $0.3\,f_c'A_g$ and $0.4\,f_c'A_g$, respectively. However, any increase in the axial load further reduced the story shears. An analogous observation can also be made in Specimen IWB2, whose story shears experienced a hike of approximately 6% and 9% when the axial load levels were

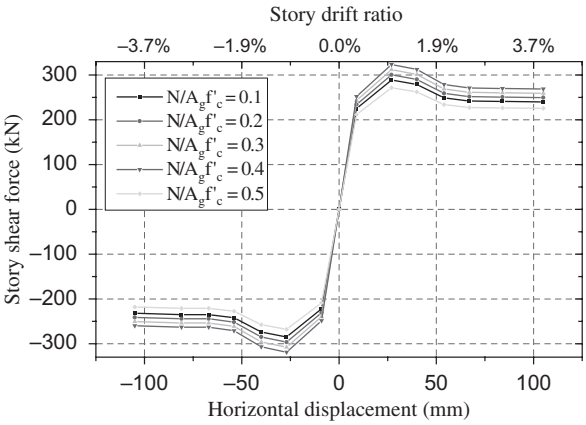

FIGURE 15 Influence of axial load variation on the story shear forces predicted by FE analysis, Specimen IWB1.

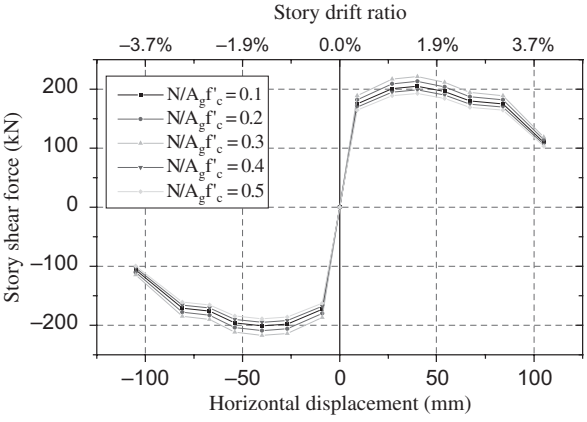

FIGURE 16 Influence of axial load variation on the story shear forces predicted by FE analysis, Specimen IWB2.

0.2 $f_c'A_g$ and 0.3 $f_c'A_g$, respectively (see Fig. 16). A further enhancement of axial load, however, led to the reduction in story shears and the degradation of stiffness. It may be observed that Specimen IWB1 carried a higher level of axial load besides achieving a greater load enhancement when compared to Specimen IWB2. This was due to its wall-like behavior which had helped to reduce the effective stresses due to the combined effect of axial compression and bending under the application of axial load. From the above discussion, it is clear that the column axial load level of 0.4 $f_c'A_g$ for Specimen IWB1 and 0.3 $f_c'A_g$ for Specimen IWB2 produced optimum enhancement in carrying story shears with values being 12% and 9%, respectively. While further increase in column axial loads beyond these specified limits reduced the strength and stiffness of the specimens.

6.2. Influence of Beam Longitudinal Bar Anchorage Ratio

Previous investigations have shown the role of beam longitudinal bar anchorage ratio in effectively transferring the shear forces and bending moments [Hatamoto *et al.*, 1991; Paulay *et al.*, 1978]. An experimental study by Hatamoto *et al.* [1991] proved that a smaller value of anchorage ratio leads to an excessive pinching of the wide beam-column joints. In a different study, Paulay *et al.* [1978] recommended that at least three-fourths of the beam longitudinal bars should pass through the column core.

In this study, the influence of beam anchorage ratio is investigated by varying these ratios in Specimens IWB1 and IWB2. Using different bar diameters and maintaining the same reinforcement area, the specimens were analyzed. The results showed no significant difference in the overall behavior of the specimens such as story shear forces and displacements at control points. Figure 17 shows the influence of beam longitudinal bar anchorage ratio on the joint shear behavior for Specimens IWB1 and IWB2. The specimens exhibited the maximum joint shear stress increase of approximately 14% when the bar anchorage ratio was enhanced to 50%.

6.3. Influence of Effective Beam Width

The slab participation in resisting the negative bending moment of wide beam joints is of great significance among the research community [LaFave and Wight, 1999; Gentry and Wight, 1994]. Because of the limited amount of test data available in literature on these topics, the effect of additional flexural capacity provided by the slabs is still not clearly

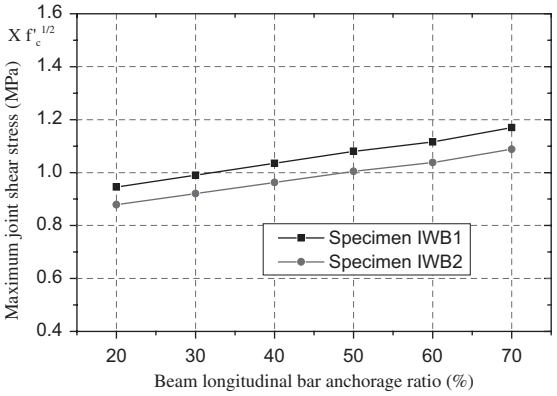

FIGURE 17 Influence of beam longitudinal bars anchorage on joint shear stress.

understood. Gentry and Wight [1994] suggested that the slab participation of wide-beam column joints might not be significant as those of non wide-beam column joints. Contrary to this, LaFave and Wight [1999] found that wide-beam column joints had a greater participation in carrying the moments compared to the conventional beam-column specimens. In addition, it was also concluded that the specimens with deep rectangular columns had larger slab participation than those with square columns. To investigate this effect, the stress and strain distributions in the wide beam were studied at critical loading cycles by varying the reinforcement in the transverse beams. The results observed at various loading cycles of Specimens IWB1 and IWB2 suggested that the value of calculated effective slab width was much lesser than the effective slab widths obtained in the FE numerical and the experimental tests. Therefore, it can be summarized that the effective wide beam width is controlled by the torsional strength of the transverse beam.

7. Conclusions

Experimental and FE numerical investigations on RC interior wide-beam column joints subjected to seismic loading are presented. Based on the results of these studies, the following conclusions can be drawn:

1. The performance of interior wide-beam column joints has been generally good in terms of the story shear forces and deformation capacities, whereas the stiffness was relatively lower compared to the normal beam-column connections. Therefore, with a suitable design criterion and proper seismic detailing, the wide-beam joints can be used to the resist lateral loadings.
2. It was noted that due to a larger section of the wide beams, the observed shear stress level in the beams was very low and therefore, the requirement of beam shear reinforcement can be relaxed.
3. The development of full-length plastic hinge in wide beams was delayed due to the lag in yielding of main bars in the beams. Due to the shear lag, the deformation angles at which all beam bars reached the yield strain was also increased. The current research showed that the part of the beam width considered effective in resisting the forces becomes smaller than the actual beam width when the beam to column width ratio is higher than 3.
4. The concrete grade did not much influence the performance the specimens. However, a further investigation can help to reveal more details.
5. A full-width plastic hinge could not develop in the specimens due to inadequate anchorage of the bars located in the outermost regions of the beams. In order to have an effective participation of the whole beam in resisting the forces, extra closed stirrups should be provided as a confinement to the outermost part of wide beam.
6. The specimens lost their loading capacity after the transverse beam lost its torsional capacity. Therefore, the transverse beam is a critical issue in the design of wide-beam systems, which needs to be carefully designed and detailed.
7. Finite element analysis results showed the influence of column axial load in the performance of the specimens. The column axial load levels of $0.4\ f_c'A_g$ in Specimen IWB1 and $0.3\ f_c'A_g$ in Specimen IWB2 were proved to be optimum in carrying story shears, with enhancements by 12% and 9%, respectively. Further increase in column axial loads, however, reduced the story shears of the specimens.
8. The finite element analysis results showed an improvement in the joint shear stress when the longitudinal reinforcement anchorage ratio is enhanced. The results indicated an enhancement by approximately 14% in the maximum joint shear stress carried by the specimens when the anchorage ratio was enhanced to 50%.

Acknowledgments

The financial assistance provided by the Protective Technology Research Centre in the School of Civil and Structural Engineering at Nanyang Technological University, Singapore is gratefully acknowledged.

References

ACI Committee 318 [2005] "Building code requirements for structural concrete (ACI 318-05) and commentary," *ACI 318R-05*, Detroit.

ACI-ASCE Committee 352 [1996] "Recommendations for design of beam-column joints in monolithic reinforced concrete structures," *ACI Manual of Concrete Practice*, part 3, ACI352R-91: 352R-1, 21.

Bonacci, J. and Pantazopoulou, S. [1993] "Parametic investigation of joint mechanism," *ACI Struct. J.*, **90**(1), 61–71.

British Standards [1997] "Structural use of concrete BS 8110, Part 1," Code of Practice for Design and Construction.

Ehsani, M. R. and White, J. K. [1985] "Effect of transverse beams, and slab on behaviour of reinforced concrete beam-column connections," *ACI Structural Journal* **82**(2), 188–195.

Hatamoto, H., Bessho, S, and Matsuzaki, Y. [1991] "Reinforced concrete wide-beam-to-column sub-assemblages subjected to lateral load," Design of Beam-Column Joints for Seismic Resistance, SP-123, J.O. Jirsa, Ed., ACI, Farmington Hills, Michigan, 291–316.

Kitayama, K., Otani, S., and Aoyama, H. [1991] "Development of design criteria for rc interior beam-column joints," Design of Beam-Column Joints for Seismic Resistance, SP-123, J. O. Jirsa, Ed., *ACI*, Farmingons Hills, Michigan, 97–123

Kulkarni, S. A., Li, B., and Yip, W. K. [2008]. "Finite element analysis of precast hybrid-steel concrete connections under cyclic loading," *Journal Construction and Steel Research* **64**, 190–201.

LaFave, J. M. and Wight, J. K. [1999] "Reinforced concrete exterior wide-beam-slab construction subjected to lateral earthquake loading," *ACI Structural Journal* **96**(4), 577–585.

LaFave, J. M. and Wight, J. K. [2001] "Reinforced concrete wide-beam construction vs. conventional construction: Resistance to lateral earthquake loads," *Earthquake Spectra* **17**(3), 479–505.

NZS3101 Concrete Structures Standard [1995] "Part-1—The design of concrete structures standards," New Zealand.

Park, R. and Paulay, T. [1975] *Reinforced Concrete Structures*, John Wiley & Sons, New York, 769 pp.

Paulay, T. and Park, R. [1984] "Joints in reinforced concrete frames designed for earthquake resistance," *Research Report 84-9*, Department of Civil Engineering, University of Canterbury, Christchurch, New Zealand, 71 pp.

Paulay, T., Park, R., and Priestley, M. J. N. [1978] "Reinforced concrete beam-column joints under seismic actions," *ACI Structural Journal* **75**(11), 585–593.

Shiohara, H. [1998] "A new model for joint shear failure of reinforced concrete interior beam," *Journal of the School of Engineering*, University of Tokyo, XLV, 16–40.

Siah, W. L., Stehle, J. S., Mendis, P., and Goldsworthy H. [2003] "Interior beam column connections subjected lateral earthquake loading," *Engineering Structures*, **25,** 281–291.

Stehle, J. S., Goldsworthy, H., and Mendis, P. [2001] "Reinforced Concrete interior wide-band beam-column connections subjected to lateral earthquake loading," *ACI Structural Journal* **98**(3), 270–279.